African Journal of Mathematics and Computer Science Research Vol. 3(8), pp.147-154, August 2010
Available online at http://www.academicjournals.org/AJMCSR

Full Length Research Paper

An adaptive finite volume method using thin plate splines for the numerical simulation of the inviscid Burgers' equation

Terhemen Aboiyar

Department of Mathematics, Statistics and Computer Science, University of Agriculture, P. M. B. 2373, Makurdi, Benue State, Nigeria. E-mail: t_aboiyar@yahoo.co.uk. Tel: 2347069121825.

Accepted 26 July, 2010

Thin plate splines are utilized in the construction of a non-oscillatory finite volume method for the inviscid Burgers' equation which is a prototype nonlinear conservation law. To capture the sharp features that occur during numerical simulation, the method is implemented on an adaptive triangulation. An a posteriori error indicator is used to detect regions where the solution varies rapidly.

Key words: Finite volume methods, WENO method, conservation laws, radial basis functions, thin plate splines.

INTRODUCTION

A wide range of problems in science and engineering are modeled with time-dependent hyperbolic conservation laws of which the inviscid Burgers' equation is a typical example. When developing numerical methods for this class of problems, care must be taken so that the presence of a discontinuity in the numerical solution does not induce spurious oscillations that affect the overall quality of the approximation. To this end, in the past few decades, a large class of high-resolution methods has been developed to handle the discontinuous solutions that are typical of hyperbolic conservation laws, while providing high order convergence rates.

Finite volume methods are well-established conservative methods for solving hyperbolic conservation laws. In general, the design of a finite volume method consists of two steps. In the first step, given initial conditions, constant, linear or high order polynomials are defined within the control volume from the cell average values of the variables. The second step involves the interface fluxes of the control volume, from which the cell averages of the variables are then obtained for a solution at the next time level (Liu et al., 2007).

Over the past few decades, the use of adaptive methods has become an integral part of many solvers for PDEs. Indeed, to enhance the quality of the numerical approximation and reduce the computational costs, especially for multidimensional problems, numerical methods may require the use of fine resolution over only some portions of the computational domain where the solution is singular (Kaser and Iske, 2005).

Essentially non-oscillatory (ENO) and weighted essentially non-oscillatory (WENO) reconstructions are used in combination with appropriate time stepping methods to obtain high order finite volume methods for hyperbolic conservation laws. The ENO method for one-dimensional conservation problems were developed by Harten et al. (1987). Two-dimensional extensions were proposed by Abgrall (1994), Harten and Chakravarthy (1991) and Sonar (1997).

In the ENO scheme, one first selects for each cell a set of stencils, each comprising a set of neighboring cells. Then, for each stencil, a recovery polynomial is computed, which interpolates given cell averages over the cells in the stencil. Amongst the different recovery polynomials, one for each stencil, the least oscillatory is selected by using a suitable oscillation indicator.

WENO schemes were developed as an improvement of ENO schemes. The WENO schemes for one-dimensional conservation laws were first proposed by Liu et al. (1994) and Jiang and Shu (1996), and were formulated in the

two-dimensional case by Friedrich (1998) and Hu and Shu (1999). In the WENO framework, the whole set of stencils and their corresponding polynomial reconstructions are used to construct a weighted sum of reconstruction polynomials to approximate the solution over a control volume of the finite volume method.

In this paper, we will utilize a WENO reconstruction using thin plate splines, a type of polyharmonic spline, on an adaptive unstructured triangular mesh. Polyharmonic splines yield flexible and numerically stable reconstruction schemes.

They are a class of radial basis functions which are powerful tools from multivariate scattered data approximation. Moreover, polyharmonic splines yield optimal reconstructions in their associated native Sobolev-type spaces called Beppo Levi spaces (Michelli and Rivlin, 1977). The semi-norm of the Beppo Levi spaces gives rise to a natural choice for the required oscillation indicator.

THE FINITE VOLUME METHOD

The 2-dimensional scalar conservation law is given as

$$\frac{\partial u}{\partial t} + \nabla \cdot F(u) = 0 \tag{1}$$

Where for Burgers' equation $F(u) = \left(\frac{u^2}{2}, \frac{u^2}{2}\right)^T$. In this paper, we will solve equation (1) numerically on a computational domain Ω with polygonal boundary and for compact time interval I subject to suitable initial and boundary conditions. The function u denotes the unknown solution of equation (1). In addition, $F(u)$ denotes the flux function, which we assume to be sufficiently smooth. For a nonlinear flux function, it is well known that the solution of the conservation law develops discontinuities, called shocks, in finite time.

When solving equation (1), we will use the finite volume method on unstructured triangulations. To this end, the computational domain Ω is partitioned through a triangulation $\boldsymbol{T}$ containing finitely many closed triangles with disjoint interior and whose union is Ω. Moreover, the intersection of two distinct triangles in $\boldsymbol{T}$ may either be empty, or an edge in $\boldsymbol{T}$, or a vertex in $\boldsymbol{T}$. This means that $\boldsymbol{T}$ is a conforming triangulation of Ω (Hu and Shu, 1999).

For any triangle $T \in \boldsymbol{T}$, the semi-discrete finite volume method is given as

$$\frac{d}{dt}\bar{u}_T + \frac{1}{|T|}\int_{\partial T} F \cdot n \, ds - 0, \qquad \text{for } T \in \boldsymbol{T} \tag{2}$$

Where

$$\bar{u}_T \equiv \bar{u}_T(t) = \frac{1}{|T|}\int_T u(t,x)\,dx, \quad \text{for } T \in \boldsymbol{T}, \quad t \in \boldsymbol{I}$$

is the cell average of u on the triangle $T \in \boldsymbol{T}$ and time $t \in \boldsymbol{I}$. In addition, n in equation (2) is the outward normal to the triangles boundary and $|T|$ is the area of the triangle.

The boundary ∂T of triangle $T \in \boldsymbol{T}$ is given by the union of three edges which we give by Γ_1, Γ_2 Γ_3, that is, $\partial T = \cup_{j=1}^{3}\Gamma_j$ so that the line integral in equation (2) can be represented as

$$\int_{\partial T} F \cdot n \, ds = \sum_{j=1}^{3}\int_{\Gamma_j} F(u(t,s)) \cdot n_j \, ds \tag{3}$$

Where n_j is the outward normal for the edge Γ_j. We discretize the integral on the right hand side of equation (3) by using a q-point Gaussian integration formula. To this end, suppose $G_1,\ldots,G_q$ and $w_1,\ldots,w_q$ denote the Gaussian points and weights for the triangle edge Γ_j. Then the Gaussian integration formula yields a high order approximation to the line integral (3) and so equation (2) becomes

$$\frac{d}{dt}\bar{u}_T + \frac{1}{|T|}\sum_{j=1}^{3}|\Gamma_j|\sum_{l=1}^{q} w_l F\left(u(t,G_l)\right)\cdot n_j - 0.$$

We then replace the terms $F(u(t,G_l))\cdot n_j$, $1 \le l \le q$, by a numerical flux function to approximate the flux across the boundaries of the neighboring triangles. In this work we will use the Lax-Friedrichs flux given by

$$F(u(t,G_l))\cdot n \approx \hat{F}(u(t,G_l))\cdot n - \frac{1}{2}\left|\left(F(u_{in}(t,G_l)) + F(u_{out}(t,G_l))\right)\cdot n - \alpha(u_{in}(t,G_l) - u_{out}(t,G_l))\right| \tag{4}$$

Where α is an upper bound for the flux function's Jacobian matrix in the normal direction n. Moreover, for time t, $u_{in}(t,G_l)$ in equation (4) is the function value of the solution's representation over triangle T and $u_{out}(t,G_l)$ is the function value of the corresponding representation over the neighboring triangle that shares the edge with T.

The finite volume method now requires us solving a system of equations

$$\frac{d}{dt}\bar{u}_T(t) = L_T(\bar{u}_T(t)) \quad \text{for } T \in \boldsymbol{T} \tag{5}$$

Where

$$L_T(\bar{u}_T(t)) = -\frac{1}{|T|}\sum_{j=1}^{3}|\Gamma_j|\sum_{l=1}^{q} w_l \hat{F}(u(t,G_l))\cdot n_j$$

The solution of this system of differential equations provides approximations to the cell averages for the triangle T at time t.

The system (5) of ODEs is solved by using a suitable Strong Stability Preserving Runge-Kutta method (SSPRK). This family of Runge-Kutta methods was first introduced by Shu and Osher

Table 1. Radial basis functions (RBFs) and their orders.

RBF	$\phi(r)$	Parameter	Order
Polyharmonic splines	r^{2k-d} for d odd	$k \in \mathbb{N}, k > d/2$	k
	$r^{2k-d} \log(r)$ for d even	$k \in \mathbb{N}, k > d/2$	k
Gaussians	$\exp(-r^2)$		0
Multiquadrics	$(1+r^2)^{\nu}$	$\nu > 0, \nu \in \mathbb{N}$	$\lceil \nu \rceil$
Inverse multiquadrics	$(1+r^2)^{\nu}$	$\nu < 0$	0

(1988). In this paper, we will use the third order SSP Runge-Kutta method given as

$$\bar{u}_T^{(1)} = \bar{u}_T^n + \Delta t L_T(\bar{u}_T^n)$$

$$\bar{u}_T^{(2)} = \frac{3}{4}\bar{u}_T^n + \frac{1}{4}\bar{u}_T^{(1)} + \frac{1}{4}\Delta t L_T\left(\bar{u}_T^{(1)}\right)$$

$$\bar{u}_T^{n+1} = \frac{1}{3}\bar{u}_T^n + \frac{2}{3}\bar{u}_T^{(2)} + \frac{2}{3}\Delta t L_T\left(\bar{u}_T^{(2)}\right)$$

Where Δt denotes the time step.

To obtain the high order spatial integration, a suitable reconstruction from current cell averages is required. Traditional methods are based on polynomial interpolation but in this paper we propose the use of polyharmonic splines, a class of radial basis functions, which we will describe in the next section. This is because, as observed by Abgrall (1994), polynomial reconstruction may lead to severe numerical instabilities.

Reconstruction of polyharmonic splines from cell averages

We will begin the discussion with the more general radial basis function method before turning to polyharmonic splines.

Given a conforming triangulation $\boldsymbol{T}$ and a triangle T, consider a stencil

$$S = \{T_1, T_2, \ldots, T_n\} \subset \boldsymbol{T}$$

of size n containing T. We now suppose that the triangles in the stencil S are associated with the functional $\{\lambda_T\}$ for $T \in S$, defined as

$$\lambda_T(u) = \frac{1}{|T|}\int_T u(x)dx, \quad \text{for } T \in \boldsymbol{T} \quad \text{and} \quad u(x) \equiv u(t,x),$$

Where for any $T \in \boldsymbol{T}$ the linear functional λ_T is known as the cell average operator for the triangle T.

Now for the given cell averages $\{\lambda_T(u)\}$ for $T \in S$ in any stencil $S \subset T$, we consider solving the reconstruction problem

$$\lambda_T(u) = \lambda_T(s), \quad \text{for all} \quad T \in S, \tag{6}$$

Where

$$s(x) = \sum_{\gamma \in S} c_\gamma \lambda_T^y(\|x-y\|) + p(x), \qquad p \in P_{k-1}^d, \tag{7}$$

is the form of the reconstruction s, $\phi: [0,\infty] \to \mathbb{R}$ is a fixed radial basis function, $\|\cdot\|$ is the Euclidean norm on $\mathbb{R}^d$ and P_{k-1}^d is the space of all polynomials in d variables of degree at most *k-1* (order *k*). In addition, λ_T^y in equation (7) denotes the action of the linear functional λ_T with respect to y, that is,

$$\lambda_T^y \phi(\|x \quad y\|) = \frac{1}{|T|}\int_T \phi(\|x \quad y\|)\, dy.$$

The order *K of P* is determined by the order $k = k(\phi)$ of the radial basis function ϕ shown in Table 1.

The reconstruction *s* in equation (7) contains *n+q* parameters, *n* for its major part and *q* for its polynomial part, but at only *n* interpolation point's conditions in equation (6). To eliminate the remaining q degrees of freedom, we solve equation (6) under the linear constraints

$$\sum_{T \in S} c_T \lambda_T(v) = 0, \quad \text{for all} \quad p \in P_{k-1}^d. \tag{8}$$

This leads to the $(n+q) \times (n+q)$ linear system

$$\begin{pmatrix} A & P \\ P^T & 0 \end{pmatrix} \begin{pmatrix} c \\ d \end{pmatrix} = \begin{pmatrix} u \\ 0 \end{pmatrix} \tag{9}$$

Where $A = (\lambda_T^x \lambda_R^y \phi(\|x-y\|))_{T,R \in S} \in \mathbb{R}^{n \times n}$; $P = (\lambda_T(x^\alpha))_{T \in S, 0 \le \alpha < k} \in \mathbb{R}^{n \times q}$ and $u = (\lambda_T(u))_{T \in S} \in \mathbb{R}^n$.

We will now focus on reconstruction with polyharmonic splines

which are due to Duchon (1977). In the polyharmonic spline reconstruction method, the radial basis function $\phi \equiv \phi_{d,k} : [0,\infty] \to \mathbb{R}$ in equation (7) is, for $d,k \in \mathbb{N}$ with $2k > d$, given by

$$\phi_{d,k}(r) = \begin{cases} r^{2k-d} & \text{for } d \text{ odd;} \\ r^{2k-d}\log(r) & \text{for } d \text{ even;} \end{cases}$$

Where *d* denotes the space dimension and *k* is the order of the basis function $\phi_{d,k}$.

The important case for us is when $d = k = 2$. This leads us to the well-known thin plate splines $\phi_{2,2}(r) = r^2\log(r)$, which is a fundamental solution of the biharmonic equation. In this case, the reconstruction s in equation (7) has the form

$$s(x) = \sum_{T \in S} c_T \lambda_T^y(\|x-y\|^2 \log|x-y\|) + d_1 + d_2 x_1 + + d_3 x_2,$$

Where we let x_1 and x_2 be the coordinates of $x \in \mathbb{R}^2$.

An important feature of the polyharmonic spline method is their optimal reconstruction property in the Beppo Levi space

$$\mathrm{BL}^k(\mathbb{R}^d) = \{u : D^\alpha u \in L^2(\mathbb{R}^d) \quad \text{for all } |\alpha| = k\}$$

which is equipped with the semi-norm

$$|u|_{\mathrm{BL}^k(\mathbb{R}^d)} = \sum_{|\alpha|=k} \binom{k}{\alpha} \|D^\alpha u\|^2_{L^2(\mathbb{R}^d)}.$$

This property says that for $\phi \equiv \phi_{d,k}$ the reconstruction $s \in \mathrm{BL}^k(\mathbb{R}^d)$ in equation (7) minimizes the semi-norm $|\cdot|_{\mathrm{BL}^k(\mathbb{R}^d)}$ among all the interpolants in $s \in \mathrm{BL}^k(\mathbb{R}^d)$ satisfying equation (6) (Duchon, 1977).

Thus, for thin plate splines, the semi-norm $|\cdot|_{\mathrm{BL}^2(\mathbb{R}^2)}$ of the corresponding Beppo-Levi space $\mathrm{BL}^2(\mathbb{R}^2)$ is for and $u \subset \mathrm{BL}^2(\mathbb{R}^2)$ given by

$$|u|^2_{\mathrm{BL}^2(\mathbb{R}^2)} = \int_{\mathbb{R}^2} \left[\left(\frac{\partial^2 u}{\partial x_1^2}\right)^2 + \left(\frac{\partial^2 u}{\partial x_1 \partial x_2}\right)^2 + \left(\frac{\partial^2 u}{\partial x_2^2}\right)^2 \right] dx_1 dx_2$$

THE POLYHARMONIC SPLINE WENO RECONSTRUCTION

Following Hu and Shu (1999), the WENO reconstruction is done as follows. For each triangle $T \in \boldsymbol{T}$ we select stencils $S = \{S_i\}$ satisfying $T \in S_i \subset \boldsymbol{T}$ for all *i*. For each stencil we compute a reconstruction s_i from $\{\lambda_T(u)\}_{T \in S_i}$ satisfying $\lambda_T(u) = \lambda_T(s_i)$. In addition, for each reconstruction s_i we compute an oscillation indicator $\mathcal{I}(s_i)$ which measures its smoothness. Fortunately for polyharmonic splines, their optimal recovery spaces, the Beppo-Levi spaces, provide a natural oscillation indicator. Thus,

$$\mathcal{I}(s_i) = |s_i|_{\mathrm{BL}^k(\mathbb{R}^d)}, \quad \text{for } s_i \in \mathrm{BL}^k(\mathbb{R}^d). \tag{10}$$

For each triangle $T \in \boldsymbol{T}$ we use the oscillation indicator to compute for each polyharmonic spline reconstruction s_i with its corresponding weight ω_i. To compute these weights we first of all compute the values

$$\tilde{\omega}_i = \frac{1}{(\epsilon + \mathcal{I}(s_i))^\rho} \qquad \text{for some } \epsilon, \rho > 0\,. \tag{11}$$

The non-negative weights of the WENO reconstruction are given as

$$\omega_i = \frac{\tilde{\omega}_i}{\sum_j \tilde{\omega}_j} \qquad \text{where} \qquad \sum_i \omega_i = 1.$$

The polyharmonic spline WENO reconstruction is thus given as

$$s(x) = \sum_i \omega_i s_i(x) \tag{12}$$

For any triangle $T \in \boldsymbol{T}$, the resulting reconstruction of *s* to *u* over *T* is used to replace *u* in the numerical flux (4), where $u_{in}(t, G_i)$ is replaced with $s_{in}(t, G_i)$ and $u_{out}(t, G_i)$ is replaced with $s_{out}(t, G_i)$.

MESH ADAPTATION

We will now describe how the WENO method can be combined with mesh adaptation. This enables us optimize computing time as well as the use of storage. The design and implementation of any adaptive method is usually guided by a suitable error indicator, which is combined with refinement and coarsening strategies for the triangular cells. We will use thin plate spline interpolation in computing an error indicator for each triangle in a triangulation $\boldsymbol{T}$ as shown in Kaser and Iske (2005). We first of all assume that each cell average $\bar{u}_T$, $T \in \boldsymbol{T}$ is assigned to the barycenter b_T of the triangle *T* that is, $\bar{u}_T \equiv \bar{u}(b_T)$. We then compute a thin plate spline interpolant of the form

$$s(x) = \sum_{T' \in \mathcal{M}(T)} c_{T'} \phi_{2,2}(\|x - b_{T'}\|) + p(x), \qquad p \in P_1^2$$

Where the barycenters $b_{T'}$ of the Moore neighbourhood $\mathcal{M}(T)$ of *T* are regarded as the interpolation points, that is, *s* satisfies the interpolation condition.

Table 2. Results for the thin plate spline WENO method for Burgers' equation.

h	$E_1(h)$	k_1	$E_2(h)$	k_2	$E_\infty(h)$	k_∞
1/8	$7.9604 \cdot 10^{-2}$	-	$6.2258 \cdot 10^{-2}$	-	$1.3799 \cdot 10^{-1}$	-
1/16	$1.8440 \cdot 10^{-2}$	2.11	$1.4125 \cdot 10^{-2}$	2.14	$3.5223 \cdot 10^{-2}$	1.97
1/32	$5.3053 \cdot 10^{-3}$	1.80	$4.3031 \cdot 10^{-3}$	1.72	$9.9759 \cdot 10^{-2}$	1.82
1/64	$1.3533 \cdot 10^{-3}$	1.97	$1.3173 \cdot 10^{-3}$	1.71	$3.2681 \cdot 10^{-2}$	1.61

$s(b_{T'}) = \bar{u}(b_{T'})$ for all $T' \in \mathcal{M}(T)$

By way of definition, for any triangle T in a conforming triangulation $\boldsymbol{T}$, the set

$\mathcal{M}(T) = \{T' \in \boldsymbol{T} : T' \cap T$ is an edge of T or a node of $T\}$

is called a Moore neighbourhood of T. Note that the Moore neighbourhood does not include T itself so that $s(b_{T'}) \neq \bar{u}(b_{T'})$. The error indicator is $\varepsilon_T = |s(b_T) - \bar{u}(b_T)|$. The error indicator $\varepsilon : \boldsymbol{T} \mapsto \mathbb{R}$ estimates the local approximation behaviour in the neighbourhood of each triangle in $\boldsymbol{T}(t)$.

For any triangle $T \in \boldsymbol{T}$, the error indicator ε_T is small, whenever the approximation quality of $\bar{u}$ by s around T is good, whereas a high value ε_T indicates that $\bar{u}$ is subject to strong variation locally around T. Thus, the error indicator allows us to effectively locate discontinuities of u quite effectively.

The error indicator is used to determine which portion of the computational mesh to refine and coarsen. The strategy we use in marking cells for refining or coarsening is summarized in the definition below.

Definition 1

Let $\varepsilon^* = \max_{T \in \boldsymbol{T}} \varepsilon_T$, and let ϑ_r, ϑ_d be two threshold values satisfying $0 < \vartheta_d < \vartheta_r < 1$. We say that a cell $T \in \boldsymbol{T}$ is to be refined if and only if $\varepsilon_T > \vartheta_r \cdot \varepsilon^*$, and T is coarsened or derefined if and only if $\varepsilon_T > \vartheta_d \cdot \varepsilon^*$. In our numerical experiments, we will use $\vartheta_r = 0.05$ and $\vartheta_d = 0.01$.

A triangle $T \in \boldsymbol{T}$ is refined by inserting its barycenter b_T as a new node of the triangulation $\boldsymbol{T}$. A cell is coarsened by removing its nodes from the triangulation. At each time step, after all the new nodes have been inserted and the nodes for coarsening have been removed, the triangulation $\boldsymbol{T}$ is updated by a local Delaunay re-triangulation. This enables an adaptive modification of the current triangulation $\boldsymbol{T}(t)$ yielding a modified triangulation $\boldsymbol{T}(t + \Delta t)$ at the next time step.

NUMERICAL EXAMPLES AND DISCUSSIONS

Example 1

We will first of all test the accuracy of the thin plate spline WENO method on the two-dimensional inviscid Burgers' equation;

$$u_t + \left(\frac{1}{2}u^2\right)_{x_1} + \left(\frac{1}{2}u^2\right)_{x_2} = 0 \qquad (13)$$

with the initial condition

$$u_0(x_1, x_2) = \frac{1}{4} + \frac{1}{2}\sin(\pi(x_1 + x_2))$$

on the computational domain $\Omega = [-1,1] \times [-1,1] \subset \mathbb{R}^2$, and with periodic boundary conditions. We carry out computations to time $t = 0.1$. The exact solution is obtained by Newton's method from the relation

$$u(x_1, x_2) = \frac{1}{4} + \frac{1}{2}\sin(\pi((x_1 - ut) + (x_2 - ut))).$$

We perform the numerical experiments on a sequence of triangular meshes of sizes $h = \frac{1}{8}, \frac{1}{16}, \frac{1}{32}, \frac{1}{64}$. The results are shown in Table 2.

We denote the numerical solution by u_h and the errors and corresponding convergence rates are computed as

$$E_p(h) = \|u_h - u\|_p \quad \text{and} \quad k_p = \frac{\log\left[\frac{E_p(h)}{E_p(h/2)}\right]}{\log(2)}, \quad \text{for} \quad p = 1, 2, \infty,$$

for the norms $\|\cdot\|_1, \|\cdot\|_2$ and $\|\cdot\|_\infty$. We implemented the method on seven stencils of size four and we

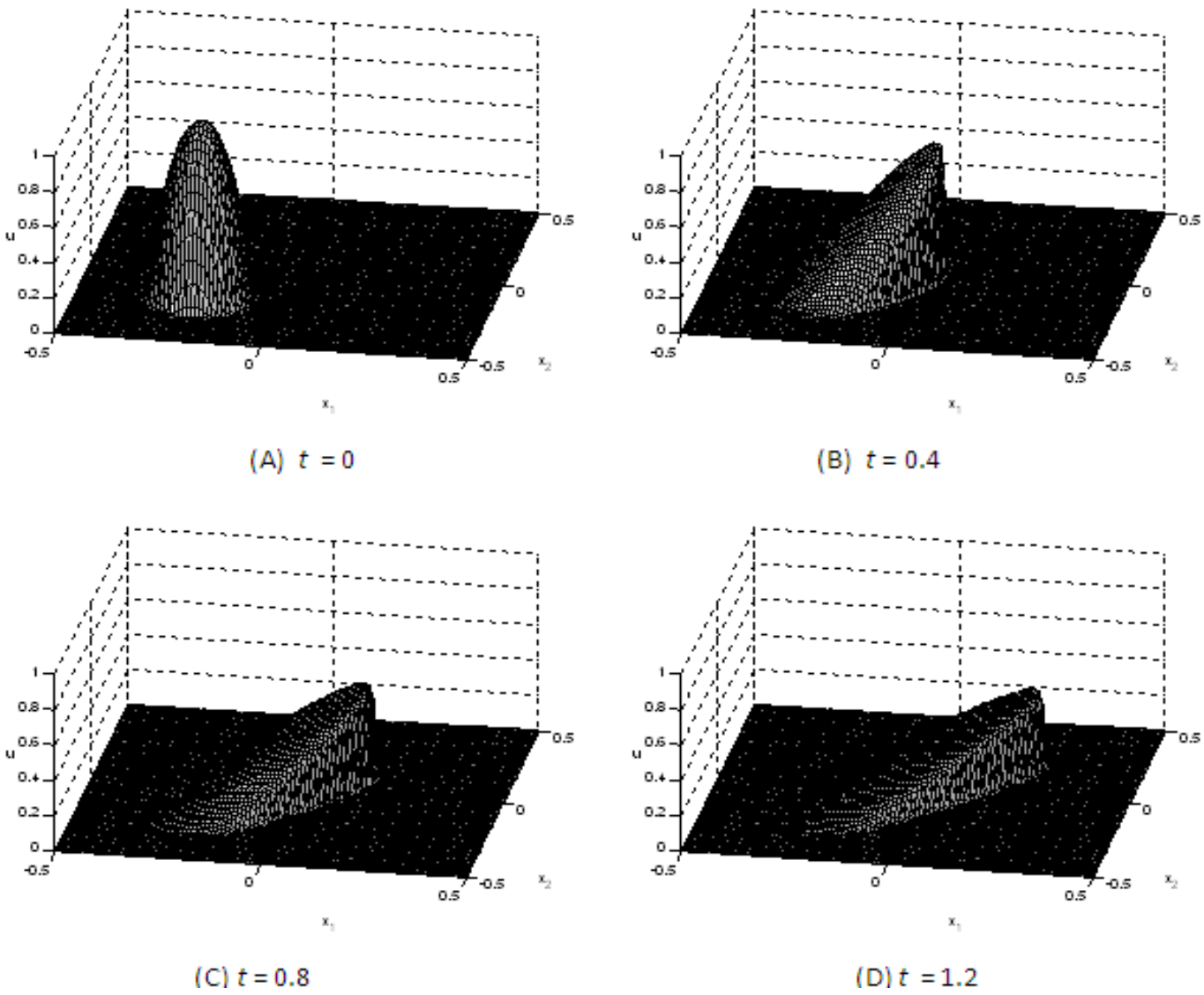

Figure 1. Solution of Burgers' equation at times (A) t = 0, (B) t = 0.4, (C) t = 0.8, and (D) t = 1.2 using the thin plate spline WENO method.

obtained a second order convergence. This agrees with the work of Iske (2003).

Example 2

In this example we look at the Burgers' equation with the initial condition

$$u_0(x_1,x_2) = \begin{cases} \exp\left(\frac{\|x-c\|^2}{\|x-c\|^2 - R^2}\right), & \|x-c\| < R, \\ 0, & \text{otherwise} \end{cases}$$

with R = 0.15, c = (-0.2, 0.2)^T on the computational domain $\Omega = [-0.5,0.5] \times [-0.5,0.5] \subset \mathbb{R}^2$. Even for smooth initial data, the solution of Burgers equation typically develops discontinuities corresponding to shocks.

We start our simulation on a base mesh of 288 triangles which we adapt to the initial conditions. The plots for the numerical solution are shown in Figure 1.

They are displayed four different times: t = 0, t = 0.4, t = 0.8 and t = 1.2. The corresponding meshes on which the numerical solution is obtained are given in Figure 2.

We notice that the initial condition, which is a Gaussian-shaped function deforms, as the simulation

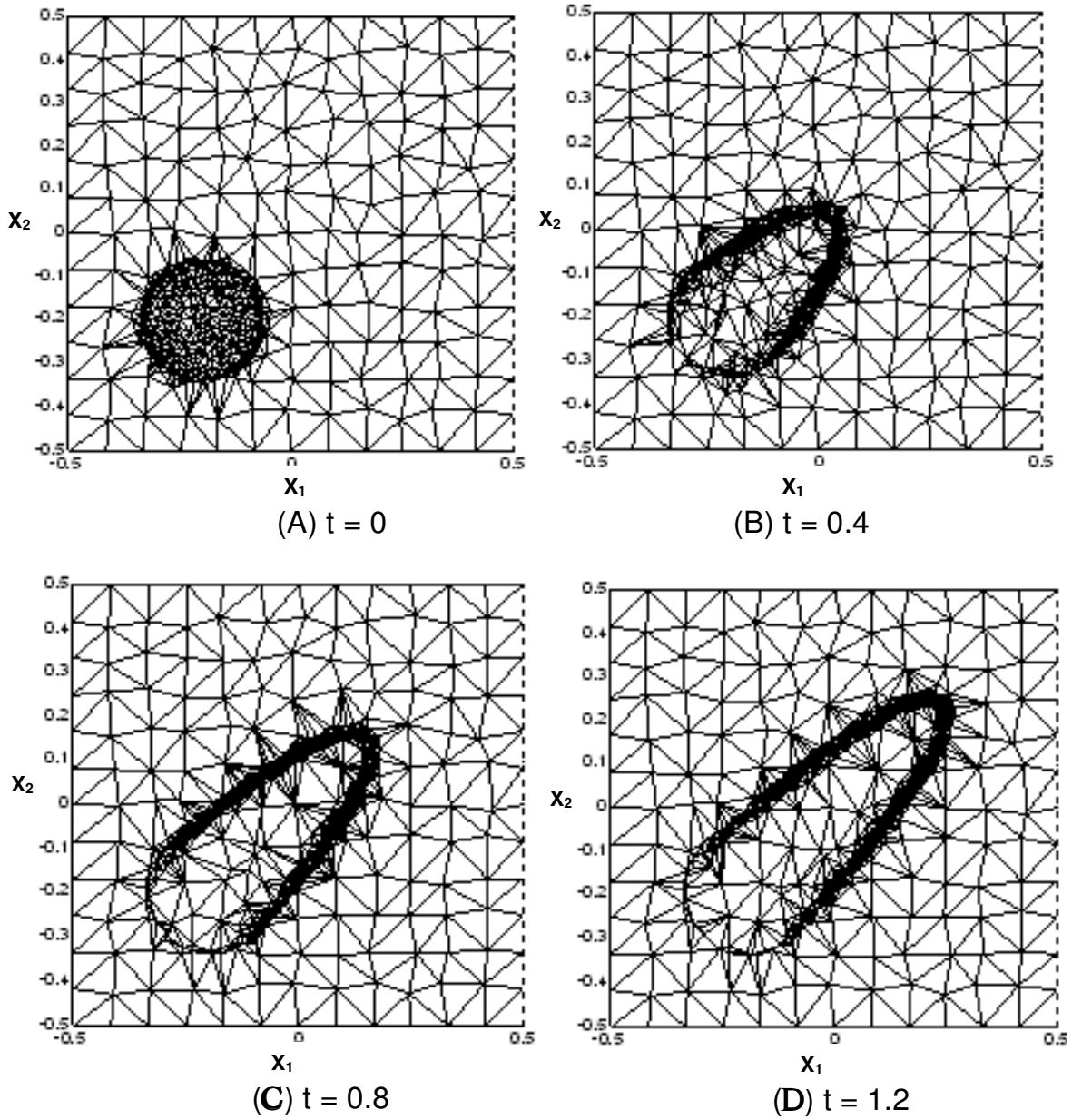

Figure 2. Adapted meshes for Burgers' equation at times (A) $t = 0$, (B) $t = 0.4$, (C) $t = 0.8$, and (D) $t = 1.2$ using the thin plate spline WENO method.

advances in time because of the nonlinearity of the Burgers' equation.

The shock is propagated throughout the simulation along the diagonal of the computational domain, and by $t = 0.8$ a very strong shock is present. The shock is however well resolved by the adaptive mesh and in regions where the solution becomes smooth, the mesh is de-refined. This confirms the effectiveness of our adaptive strategy.

REFERENCES

Abgrall R (1994). On ENO schemes on unstructured meshes: analysis and implementation, J. Comp. Phys., 114: 45-58.

Duchon J (1977). Splines minimizing rotation invariant semi-norms in Sobolev spaces, In: Schempp W, Zeller K (eds), Constructive Theory of Functions of Several Variables, Springer- Berlin, pp. 85-100.

Friedrich O (1998). Weighted essentially non-oscillatory schemes for the interpolation of mean values on unstructured grids, J. Comp. Phys., 144, 194-212.

Harten A, Chakravarthy SR (1991). Multidimensional ENO Schemes for

General Geometries, ICASE Report 91-76.
Harten A, Engquist B, Osher S, Chakravarthy SR (1987). Uniformly high order accurate essentially non-oscillatory schemes III, J. Comp. Phys., 71: 231- 303.
Hu C, Shu CW (1999). Weighted essentially non-oscillatory schemes on triangular meshes, J. Comp. Phys., 150: 97-127.
Iske A (2003). On the approximation order and numerical stability of local Lagrange interpolation by polyharmonic splines. In: Haussmann W, Jetter K, Reimer M and Stockler J (eds), Modern Developments in Multivariate Approximation, International Series of Numerical Mathematics, Birkhauser, Basel, pp. 153-165.
Jiang GS, Shu CW (1996). Efficient implementation of weighted ENO schemes, J. Comp. Phys., 126: 202-228.
Kaser M, Iske A (2005). ADER schemes on adaptive triangular meshes for scalar conservation laws. J. Comp. Phys., 205: 486-558.
Liu XD, Osher S, Chan T (1994). Weighted essentially non-oscillatory schemes. J. Comp. Phys., 115: 200-212.
Liu Y, Shu CW, Tadmor E, Zhang M (2007). Non-oscillatory hierarchical reconstruction for central and finite volume schemes, Comm. Comp. Phys., 2: 933-963.
Shu CW, Osher S (1988). Efficient implementation of essentially non-oscillatory shock capturing schemes. J. Comp. Phys., 77: 439-471.